

Two-Photon Polymerization of Soft Matter Composites

by

Yasser A. Albarakat

B.S., Engineering Physics, University of Colorado Boulder

B.S., Applied Mathematics, University of Colorado Boulder

Defense Date: 04/06/2017

Reserach Adviser: Ivan Smalyukh (Physics)

Honors Council Representative: Paul Beale (Physics)

Committee Member: Bengt Fornberg (Applied Mathematics)

A thesis submitted to the
Faculty of the Honors Program of the
University of Colorado Boulder in partial
fulfillment of the requirements for
graduation with Latin honors for the degree of
Bachelor of Science
Department of Physics

2017

This thesis entitled:
Two-Photon Polymerization of Soft Matter Composites
written by Yasser A. Albarakat
has been approved for the Department of Physics

Ivan Smalyukh

Paul Beale

Bengt Fornberg

Date _____

The final copy of this thesis has been examined by the signatories, and we find that both the content and the form meet acceptable presentation standards of scholarly work in the above mentioned discipline.

Albarakat, Yasser A. (B.S., Engineering Physics)

Two-Photon Polymerization of Soft Matter Composites

Thesis directed by Ivan Smalyukh

With two-photon photopolymerization (2PP), it is possible to design and produce composite materials with three dimensional control and sub-micron precision, thanks to highly localized nonlinear process of polymerization [24]. In this work, the feasibility of fabricating mesostructured composite particles with pre-defined shape and topology is examined. We explored polymerizable materials from both commercial sources and laboratory products as well as variable laser parameters, including pulse width and intensity along with dwell time, to find optimum conditions for 2PP. Later 2PP was performed on polymerizable materials containing quantum dots dispersion and the optical response of the resultant composite was characterized with spectroscopy. In addition to regular isotropic photopolymers, elastomers with liquid crystal phase were also studied, paving the way for engineering composite materials with anisotropic thermomechanical responses.

Dedication

To family and friends.

Acknowledgements

I would like to take this chance to thank Professor Ivan Smalyukh for giving me this opportunity, and for all the support and guidance he has been providing. I am grateful for Ye Yuan and Benny Tai. Ye has been a great mentor since the first day I joined the group. I learned from him almost all of what is presented in this thesis. I would not have done a large portion of this thesis without the help of Benny. He helped me understand my project better, and he was there for me at a time when I needed assistance. Also, I am grateful for Dr. Qingkun Liu, Dr. Taewoo Lee, Dr. Haridas Muntoor, Andrew Hess, and all the other great group members for all the help they provided.

I would like to express my gratitude to KAUST Gifted Student Program (KGSP) for not only giving me the opportunity to pursue higher education in the United States, but also encouraging me to participate in undergraduate research opportunities. I would also like to thank the Undergraduate Research Opportunities Program (UROP) for sponsoring part of my research.

Contents

Chapter	
1	Introduction 1
2	Background 2
2.1	Liquid Crystals 2
2.2	Quantum Dots 4
2.3	Polymerization Materials 5
2.4	Structure of Polymerization Microparticles 7
3	Methods 9
3.1	Sample Preparation 9
3.2	Mixture Preparation 11
3.3	Microscopy 11
3.4	Two-Photon Polymerization 14
3.4.1	Principles 14
3.4.2	Apparatus and Setup 15
4	Results and Discussions 19
4.1	Polymerization with Stretched Pulse 21
4.2	Polymerization with an Ultrafast Pulse 24
4.3	Composite Polymerization with Cadmium Telluride Quantum Dots 27

4.4	Elastomer Polymerization	30
4.4.1	Preparation	30
4.4.2	Experiment	32
5	Conclusions	34
	Bibliography	37

Tables

Table

3.1	Relation between pixel dwell time in program settings and measured dwell time plus response time (inter-pixel travel)	18
-----	---	----

Figures

Figure

2.1	Nematic liquid crystal orientational order	3
2.2	Liquid crystal defect	4
2.3	Quantum dots	5
2.4	Polymerization process	6
2.6	Hopf link structure	7
2.5	Liquid crystal elastomers	8
3.1	Preparing substrates and cover glass	10
3.2	Microscopy setup	13
3.3	Comparison between one and two photon polymerization.	14
3.4	Two-photon polymerization setup	16
3.5	Two-photon polymerization setup	17
4.1	Polymerization regions	20
4.2	Polymerization regions for LCEs	21
4.3	Stretched pulse	22
4.4	Polymerization with stretched pulse.	23
4.6	NOA 63 polymerization	26
4.7	Energy threshold	27
4.8	Resin fluorescence	28

4.9 QDs fluorescence	29
4.10 Emission spectra	29
4.11 LCEs heated over night	31
4.12 LCE overnight alignment	32
4.13 LCE polymerization regions	33
5.1 Polymerization regions for a pixel dwell time of 0.00075 s	36

Chapter 1

Introduction

Composite materials, as common as concrete, have been widely used and extensively engineered due to their capability of combining constituent materials with significantly different physical or chemical properties, generating new materials with novel and more desirable properties. Recent interest in composite materials includes specialized alloy to meet the demand of aerospace applications [25], integration of sensing and communicating modules into composites [21], and fabrication of core-shell nanostructures [16]. With two-photon photopolymerization (2PP), it is possible to design and produce composite materials with three dimensional control and sub-micron precision, thanks to highly localized nonlinear process of polymerization. In this work, we explored polymerizable materials from both commercial sources and laboratory products as well as variable laser parameters to find optimum conditions for 2PP. Later 2PP was performed on polymerizable materials containing quantum dots dispersion and the optical response of the resultant composite was characterized with spectroscopy. In addition to regular isotropic photopolymers, elastomers with liquid crystal phase were also studied, paving the way for engineering composite materials with anisotropic thermomechanical responses.

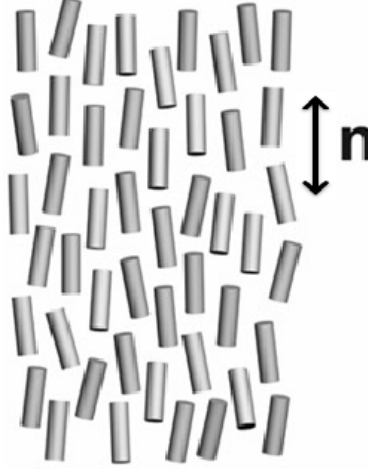
Chapter 2

Background

2.1 Liquid Crystals

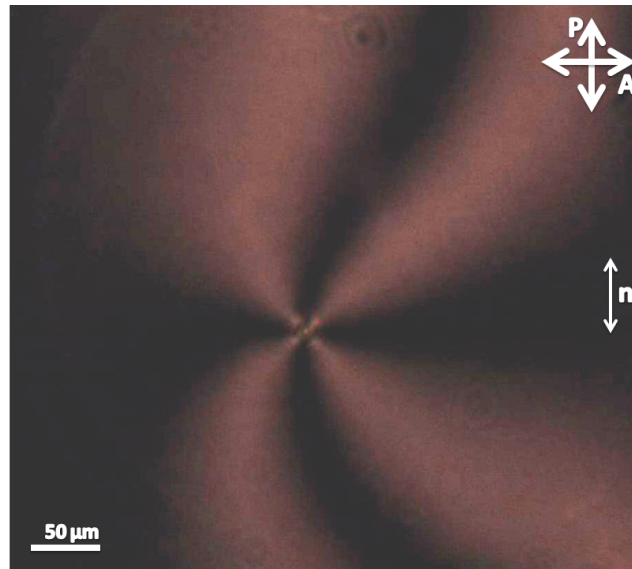
Liquid crystals (LCs) are a form of matter that is in between isotropic liquid and anisotropic crystalline. Their constituent molecules often take the shape of rods and possess orientational but not all the spatial ordering, while macroscopically they can flow, drip and take the shape of their container like a fluid. A typical LC molecule, 4-cyano-4-pentylbiphenyl (5CB), is about 1.8 nm long with a diameter of 0.5 nm [27]. The simplest phase of LC is nematic, where all molecules point roughly towards the same direction but are positioned randomly (Fig. 2.1). Other phases such as smectic or cholesteric may exhibit more complex orientation ordering or partial spatial ordering. LC phases exist in a relatively narrow temperature range. As temperature increases, LCs become less ordered and when the temperature exceeds a certain limit, known as the clearing temperature T_c , LCs become completely isotropic. An example is 5CB exhibiting nematic phase in room temperature with a clearing point of $T_c \approx 35^\circ\text{C}$.

Figure 2.1: Nematic liquid crystal orientational order. The director of LCs field is pointed by \vec{n} . Due to non-polar ordering of LCs, $\vec{n} = -\vec{n}$ [27].



The orientation ordering of LC molecules can be described by so-called director field $\vec{n}(r)$ defined as the local average of molecular orientation. Different from a vector field such as electric or magnetic field, director is non-polar $\vec{n} = -\vec{n}$, given the non-polar nature of LC molecular interaction. The symmetry-breaking due to orientation ordering of LC results in anisotropic properties. For example, the refractive index experienced by light polarized parallel to the director is different from that of light polarized perpendicular to the director. The former index is known as extraordinary refractive index and the latter is the ordinary refractive index. Therefore, under polarizing optical microscopes, LCs often show colored patterns corresponding to different molecular orientation (Fig. 2.2).

Figure 2.2: Liquid crystal defect (Schlieren texture).



2.2 Quantum Dots

Quantum dots (QDs) are semiconductor nanocrystals that are only a few nanometers in size. When excited by electricity or light, QDs can emit light of specific frequencies that can be tuned by changing their size. Similar to atoms, this fluorescence comes from discrete energy levels due to confinement of electrons imposed by the size of QDs. As the size of the QDs increases, the bandgap decreases, and the emitted color is redshifted. This is to say that small QDs tend to emit blue light while large ones emit red [34]. The quantum dots used in this work are Cadmium telluride (CdTe) QDs. They are obtained by chemical synthesis [19]. Figure 2.3 shows synthesized QDs with different sizes.

Figure 2.3: Synthesized CdTe QDs with different sizes.

Quantum dots (CdTe, 2-6 nm): size-tunable bandgap



The tunability of the optical response of QDs allows for a variety of applications ranging from tunable gain medium for random lasers, to bio-imaging and qubit candidacy in quantum computations [14]. Lasers that use QDs as a gain medium have the advantage of easily tuning the gain wavelength by simply tuning the size of QDs. This tunable medium could in turn lead to low lasing threshold. Furthermore, QDs have promising applications in biophysical and tissue sciences. This promise is captured in deep penetrative bio-imaging and disease diagnostics. The QDs imaging approach complement fluorescence microscopy [31].

2.3 Polymerization Materials

Polymerization of three different photo-polymerizing materials are discussed in this work: Norland Optical Adhesive 63 (NOA63), Formlabs FLGPCL02 Clear resin, and liquid crystal elastomers.

Norland Optical Adhesive 63 (NOA 63) is a commercially available UV-curable glue with an absorption peak at 350-380 nm. It looks colorless and transparent due to its high transmission in the visible region. The recommended energy for full cure is 4.5 Joules/sq. cm and the refracted index of cured polymer is 1.56 [23]. NOA 63 works exceptionally as an UV-curable glue. However, it does not polymerize well in our 2PP system at 780 nm. Nonetheless, 2PP results of NOA 63 are shown and compared to that of other materials in this work.

Formlabs FLGPCL02 Clear resin is also commercially available transparent resin, designed to be used with Formlabs 3D printer. It can be polymerized by illumination of at 405 nm. Formlabs

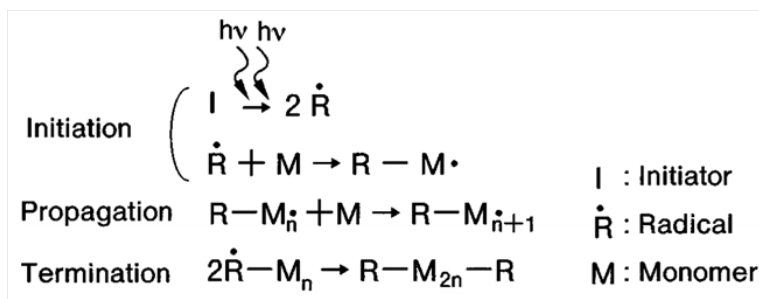
resin is not a good 2PP material as it is at 780 nm. We mixed Formlabs with a photo-initiator, Irgacure 369, in order to make it two-photon polymerizable at 780nm, which is the excitation wavelength used in our 2PP setup.

Liquid crystal elastomers (LCEs) are a type of elastomers that have anisotropic properties. Elastomers are made of polymeric chains that have elastic properties. These chains give rise to macroscopic properties. Elastomers can be stretched by applying a force, and they return to the original configuration in the absence of this force.

Elastomer chains consist of linked segments known as monomers. Elastomers are created when different monomer chains connect using crosslinkers (see Figure 2.5a). The elasticity of elastomers come from those crosslinkers since they act like springs in the sense that they represent a restoring force.

The polymerization process is summarized in Figure 2.4. The process starts when photo-initiators absorb photons and break to form radicals. These radicals combine with monomers to form radical chains. The radical chains grow by combining with more monomers. This process terminates when two radical chains come together.

Figure 2.4: Summary of the polymerization process.



In LCEs, each chain consists of mesogens connected to it, as depicted in 2.5b. Mesogens are aligned in a similar fashion as liquid crystals, giving LCEs anisotropic properties. What makes LCEs especially interesting is their thermomechanical response. When LCEs are heated, orientational

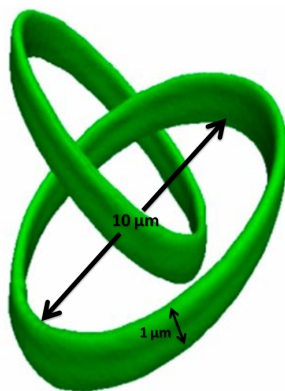
order inside LCEs chains disappears. Elastomers then compress in the direction parallel to the director of the liquid crystal field, and they stretch in the perpendicular direction. Other non-LC elastomers, on the other hand, compress and stretch isotropically [18].

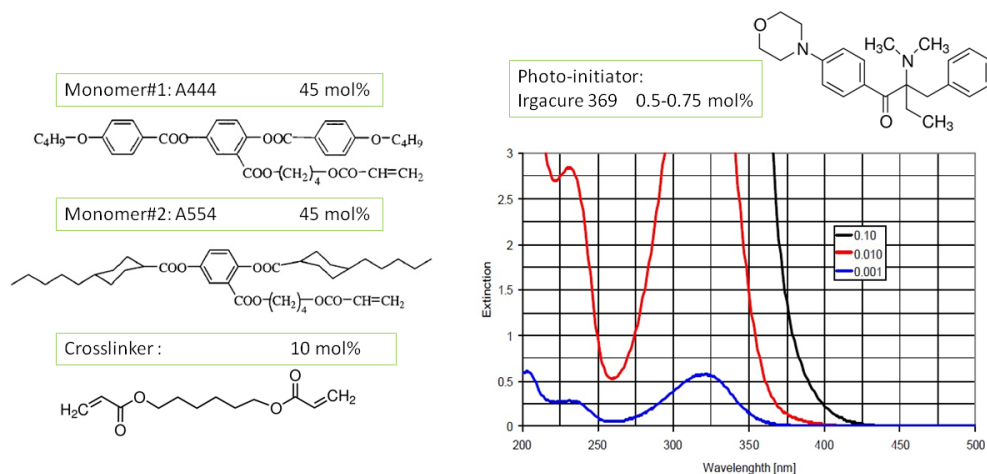
In contrast with the first two polymerizable materials, the used LCEs are prepared in the lab and have been optimized for alignment with polyimide SE 1211, a polymer used to coat the surface of substrates and cover glass. The chemical structure of LCEs is shown on Figure 2.5a.

2.4 Structure of Polymerization Microparticles

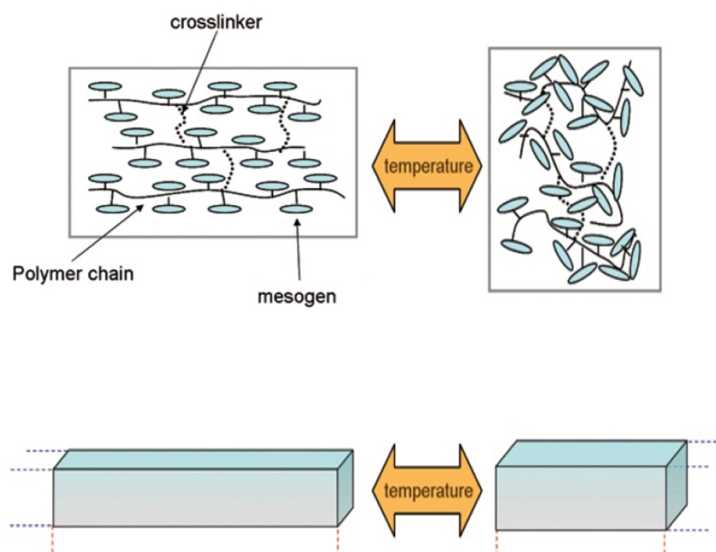
A hopf link consists of two tori linked together only once. This structure is chosen for this study. What makes it special is that it is a nontrivial topology, and yet, it is relatively simple. These facts make hopf link good candidate to investigate polymerization regions. The diameter of the torus used in the hopf link structure is $10 \mu m$, and the inner diameter is about $1 \mu m$ (Fig. 2.6).

Figure 2.6: Hopf link structure[1].





(a) LCE material composition: Mixture of monomers, crosslinker and photo-initiator. The plot shows excitation wavelength for different concentration of photo-intisiators. For the prepared LCEs, the concentration of photo-initiator used is about 0.7%, so excitation peak lies in the UV range, somewhere between the red and blue curves. [7].



(b) Thermomechanical response of LCEs: During heating, a transition from LCE phase to isotropic phase takes place. This change stretches LCEs in the perpendicular direction to the director and compresses LCEs in the parallel direction. During cooling, the opposite process occurs.

Figure 2.5: Liquid crystal elastomers

Chapter 3

Methods

3.1 Sample Preparation

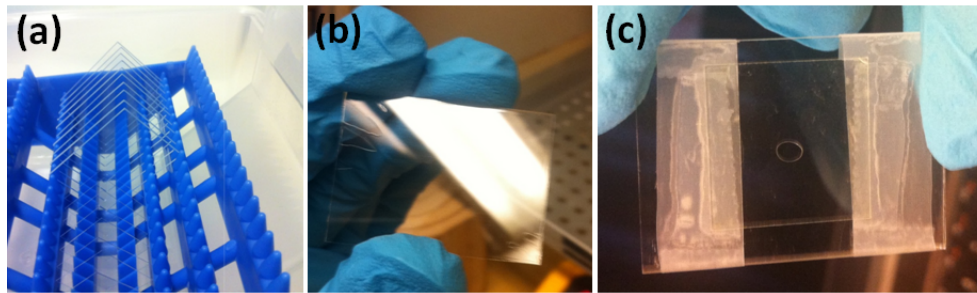
A 2PP sample is composed of a substrate, a cover glass, and a droplet of polymerizable material in between. The dimensions of used substrates and coverslips are 25.4 mm×34 mm and 18 mm×18 mm respectively. The thickness of the coverslip is about 150 μm . Using a thin cover glass is essential in the 2PP process since the objective used to focus the laser beam requires a short working distance. A barrier is needed to separate immersion oil from the polymer droplet. Both substrates coverslips are available commercially. Those used in this report are bought from Fisher Scientific.

The preparation process of a sample consists of three major steps: Washing substrate and cover glass, setting boundary conditions, and cell construction. A detailed description of each of those steps is provided below.

Glass treatment starts with washing. The tray containing the glass is put in a sonicator water bath. To clean the glass, detergent is added. The tray should be sonicated in the bath for at least 30 minutes at a temperature of 50°C. The tray should not leave the bath until the temperature drops to below 35°C. Right after removing the tray from the bath, the glass must be rinsed well with 1L of deionized (DI) water, and 500 mL of each of the following organic solvents: acetone, methanol, and isopropanol. DI water and solvents must be prepared in advance. The glass should not dry out before the end of the rinsing process. When the process is finished, the tray can then be left in a controlled environment to dry. The result of this process is clean glass as shown in

Figure 3.1a.

Figure 3.1: Preparing substrates and cover glass: (a) Substrates and cover glass after washing. (b) A substrate coated with a polymer. The edges of the polymer are shown. (c) Cell construction.



The second step of the sample preparation process is to set boundary conditions (BCs). This step only applies for samples that use anisotropic materials like LCEs. Surface of one side of glass is coated with a polymer. The polymer used in this study is Polyimide SE 1211. This is done by placing about $50\mu L$ of the polymer on the center of glass. Then, the polymer is distributed all over the glass by spin coating. The spin coating speed is 3000 rpm for 30 seconds. Right after the spin coating is performed, substrates and cover glass are placed on a hot plate at $110^{\circ}C$ for approximately three minutes, and then they are put in an oven at a temperature of $185^{\circ}C$ for one hour. This process creates a thin film on glass. The boundary conditions set in this study are homeotropic. For LCEs, this means that they are aligned perpendicular to the substrate. There are a wide range of thickness depth that can be set. The used thickness is $100\mu m$. This is the separation between substrate and cover glass. It is set by a Scotch tape as shown in Figure 3.1c. Once the thickness is determined, a droplet of polymer is sandwiched between a substrate and a cover glass. The final step is to bind the glasses by scotch tape.

3.2 Mixture Preparation

There are three preparation procedures discussed in this section: mixing Formlabs polymerizable material with photo-initiators, PEG surface treatment of QDs, and mixing QDs with Formlabs polymerizable material. NOA 63 does not require special handling, and the preparation of LCEs is discussed in the results chapter since it is not a well established method.

As mentioned in chapter 2, Formlabs polymerizable material requires addition of photoinitiators. The photoinitiator used is Irgacure 369. Mixture is achieved by stirring and sonication in boiling water.

Before using CdTe QDs, a Polyethylene glycol (PEG) surface treatment is done to ensure that QDs mix well with polymerizable material. PEG is bought from JenKem Technology. The first step of this process is to separate QDs from their original solvent, water in this case, by centrifuging around 5 krpm, and mix them with a solvent. Then, about 10 mg of PEG is dissolved in 2 mL of the solution. After 24 hours, QDs are separated again from the mixture and placed in methanol.

Once the QDs are uniformly distributed in methanol, the next task is to mix the QDs uniformly with a polymerizable material. Several methods have been tried, and the most effective one so far is done by adding QDs solvent mixture to polymerizable material, and stirring this final mixture overnight at high speed. Centrifuging may be needed to spin down large clusters of QDs.

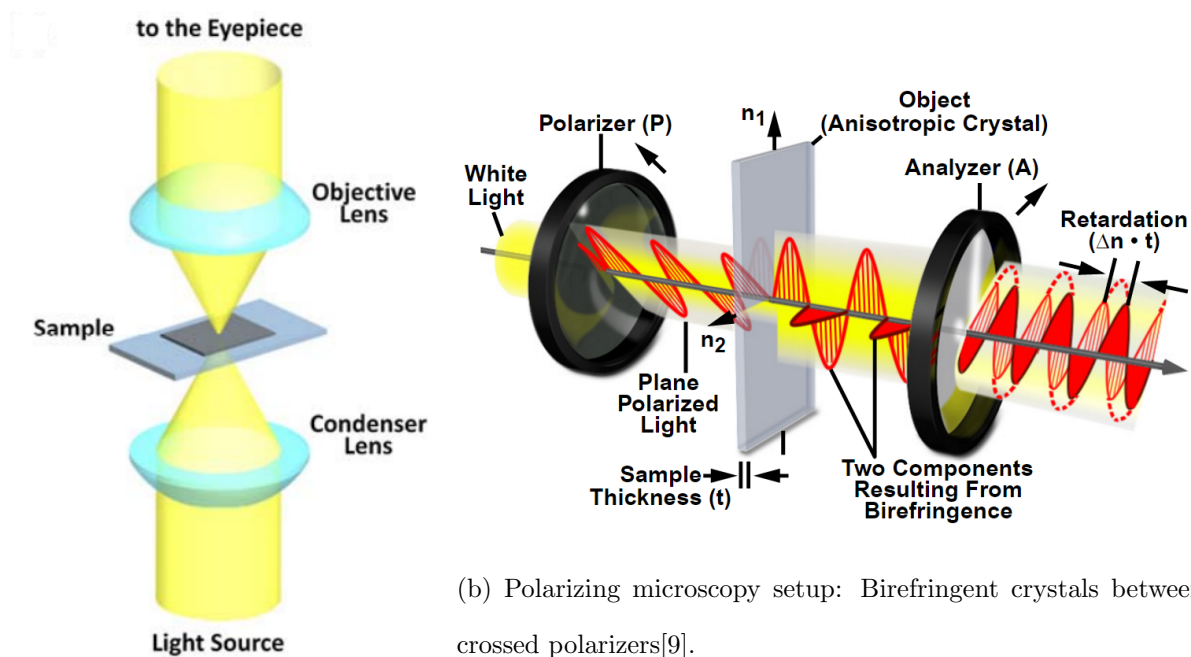
3.3 Microscopy

There are three microscopy methods used in this study. Before embarking on outlining those methods, it is essential to explain numerical aperture (NA). This is a dimensionless parameter that describes the angles over which an objective "sees" light. To optimize image resolution, NA of the objective should be equal to that of the condenser. Optimizing image contrast, on the other hand, requires NA of the objective to be higher.

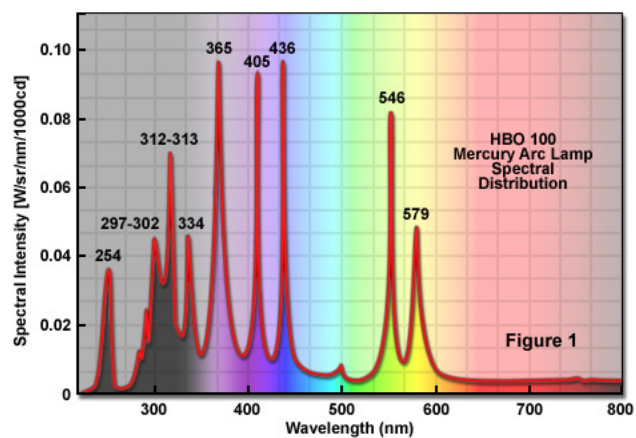
Bright field microscopy is the simplest and most common microscopy. As shown in Figure 3.2a, unpolarized light is focused in the sample by a condenser lens. The image is constructed by

the interaction between incident light and the sample. This interaction could include absorption, refraction, scattering, and reflection. One drawback of using this imaging method is poor contrast when samples have weak spatial variation of the refractive index [30].

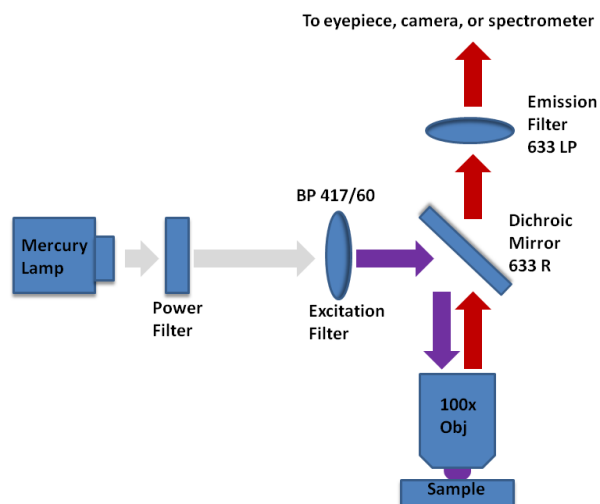
Polarizing microscopy, also known as crossed polarizers microscopy, is used to measure birefringence. As shown in Figure 3.2b, incident white light is polarized along the direction of a polarizer. This polarized light is then used as the illumination source for the sample. If the sample has no birefringence, then the polarization of the light would not change, and the analyzer would block all of the light. However, if there is a birefringence, then the incident light polarization would change. This suggests that the component that is along the analyzer direction would pass to the eyepiece.



(a) Bright field microscopy setup.



(c) Mercury lamp spectrum [8].



(d) CdTe QDs emission measurement setup

Figure 3.2: Microscopy setup

The last microscopy setup used in this paper is the setup to measure CdTe QDs optical response. To construct this setup, it is essential to mention that the QDs emission wavelength is

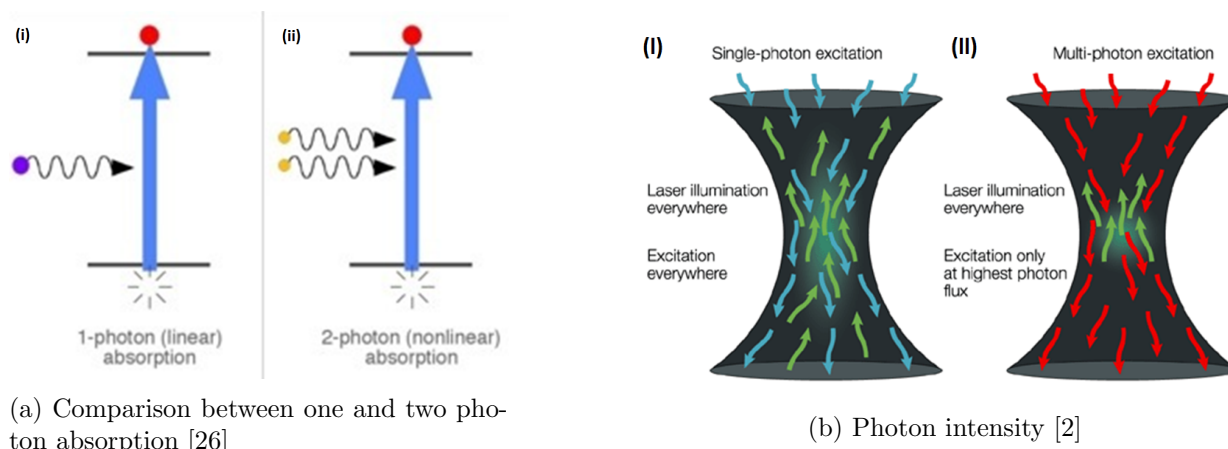


Figure 3.3: Comparison between one and two photon polymerization.

around 700 nm, the absorption wavelength is in the UV range and it is expected to be around 400 nm, and the excitation source used is a mercury lamp (see spectrum 3.2c). A band-pass excitation filter, as shown in figure 3.2d, is used to select an excitation wavelength of 417 nm with a width of 60 nm. This means that photons in the range of 387 nm to 447 nm from the mercury lamp would pass through the excitation filter and excite the QDs. The excitation beam is then reflected toward the sample by a 633 nm dichroic mirror. It is focused using a 100x objective into the sample. The emission response is then collected from the sample by this objective. Since the emission is around 700 nm, it would pass through the dichroic mirror and a long pass filter of 633 nm, making its way to the eyepiece.

3.4 Two-Photon Polymerization

3.4.1 Principles

Two-photon polymerization (2PP) is a common technique used to implement micro-scale topologies. It applies a focused femtosecond laser pulse to a light sensitive material, which causes it to polymerize. This method uses a two-photon approach, and hence the name.

2PP offers the spatial resolution needed to "print" specific shapes. 1PP would polymerize a cone, while 3PP would be more accurate, but it requires higher powers to polymerize (Fig.

3.3b). 1PP can be used to print 2D pattern like chip manufacturing. An approach realizing three-dimensional microfabrication based on two-photon polymerization with ultrafast laser pulses has been widely studied and implemented. When ultrafast laser pulses with high peak intensity are focused into a volume of polymerizable material, two-photon polymerization is initiated through two-photon absorption and subsequent polymerization. After illumination of the pre-designed structure inside the volume of polymerizable material, non-illuminated, and non-polymerized, material is washed away, and the polymerized material remains in the prescribed 3D structure. With a suitable ultrafast laser source and some control system, micro-fabrication of any computer generated 3D structure is possible by direct laser writing.

2PP fabrication makes use of the nonlinear multi-photon nature of two-photon absorption to achieve localized excitation the ensuing resolution in 3D. When two-photon absorption happens, two photons arrive simultaneously and combine their energies to excite the molecule to an excited state (Fig. 3.3a). Nonlinear processes require much higher intensities of excitation than linear processes.

3.4.2 Apparatus and Setup

The laser source used in 2PP is a mode-locked tunable Ti-sapphire femtosecond laser (Chameleon Ultra II, Coherent), emitting 140 fs pulses at a repetition rate of 80 MHz. Since the polymerizable materials can be excited at 390 nm in a single photon process, the wavelength of used laser is 780 nm. The laser beam path is illustrated by Figure 3.4. Laser is focused by an Olympus 100 oil-immersion objective with NA of 1.4. The 2PP system is placed on a smart optical table to prevent undesired vibrations that may affect the quality of the polymerized structure.

Figure 3.4: Two-photon photopolymerization of chiral microparticles. (a), A schematic of the home-built two-photon photopolymerization setup showing its key components. A LabVIEW-based computer software controls timing between the fast shutter and the nano-positioning stage in order to draw desired structures of the photopolymerized solid microparticles. The inset shows a schematic representation of the photopolymerization cell with monomer and photoinitiator in the form of a droplet sandwiched between a glass slide and a microscope coverslip of $170\ \mu\text{m}$ in thickness; translation of the focal point of the focused laser beam within the cell yield chiral microparticles with different handedness. GLP is the Glann laser polarizer, HWP is the half-wave plate, and DM is a dichroic mirror. Adopted from [33]. (b),(c) show the capabilities of the 2PP system. 3D micro-printing with direct laser writing [20].

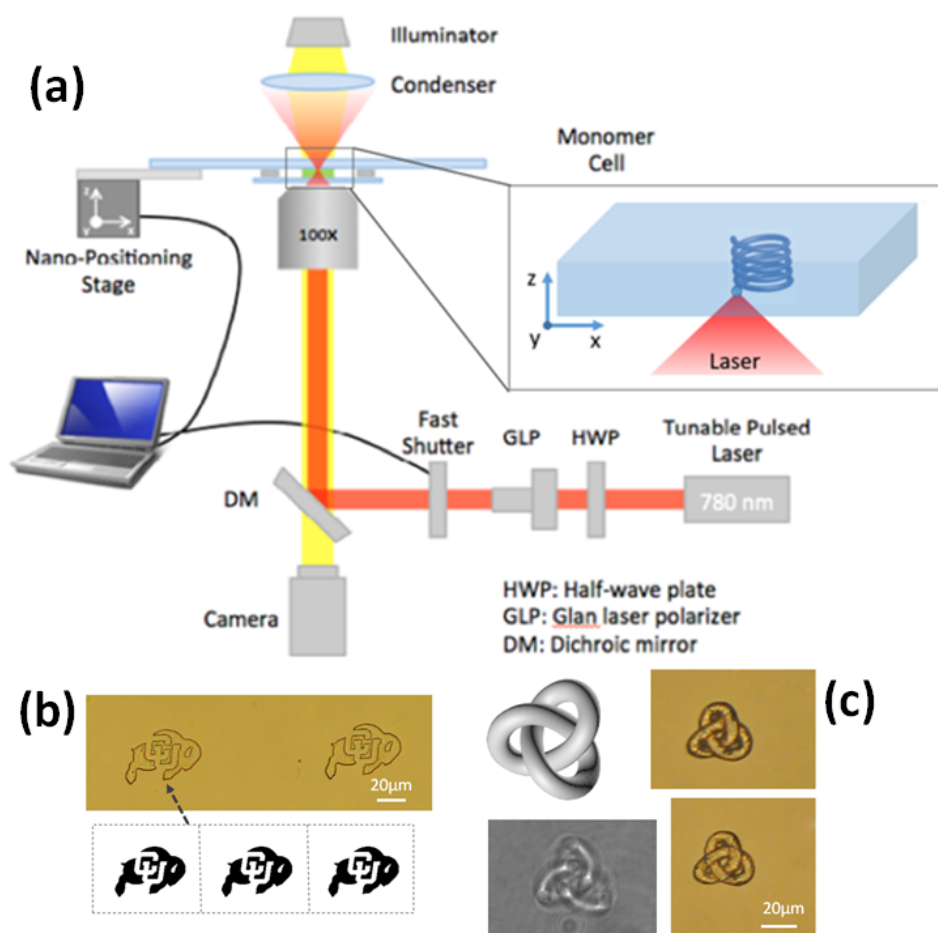


Figure 3.5: 2PP setup

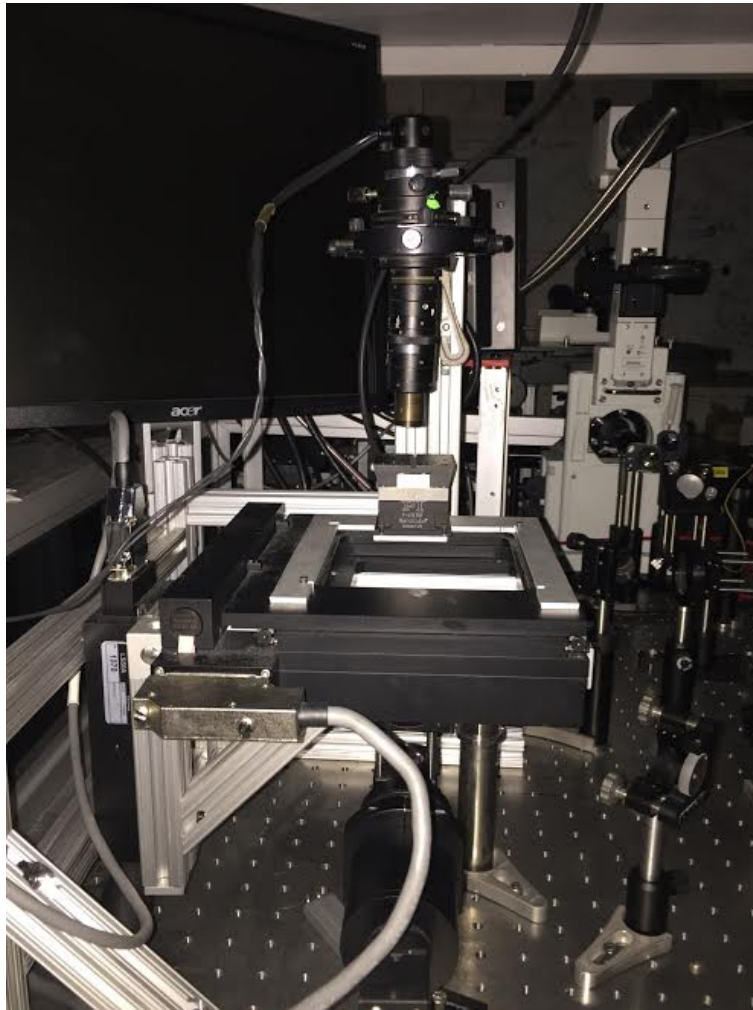


Table 3.1 compares between the pixel dwell time parameter inserted in the LabVIEW program used in 2PP control and the actual measured dwell time plus a response and inter-pixel travel time. This explains why the measured time is larger than that of program settings time. The effect of response/travel time is most significant when dwell time is short. It is imperative to state that the dwell time used in the results chapter is program settings dwell time.

Table 3.1: Relation between pixel dwell time in program settings and measured dwell time plus response time (inter-pixel travel)

<i>Dwell Time in Program Settings*</i> (sec)	<i>Measured Dwell and Response Time (inter – pixel travel)[†]</i> (sec)
0.00075	0.0077
0.01	0.016
0.02	0.035
0.03	0.071
0.05	0.108
0.1	0.210

*Program settings dwell time is a parameter inserted in the LabVIEW program. It controls pixel dwell time used in the 2PP stage.

[†]Measured time includes dwell time and response and travel between pixels time.

Chapter 4

Results and Discussions

Three main studies are performed: dependence of two-photon photopolymerization (2PP) on laser pulse width, polymerization of composite material with QDs, and LCE alignment and polymerization.

Before discussing the results, it is essential to list the criteria used for the characterization of polymerization areas. For NOA 63 and Formlabs resin, there are four polymerizable areas, as seen in Figure 4.1. In the first region represented in yellow color¹, no polymerization is observed, indicating that in this region the laser power is too low to initiate the polymerization process. The next cyan region is where laser power is increased and polymerization can be observed. However, the polymerized structures are not strong enough. They may be dissolved in the process of removing unpolymerized material with organic solvents (isopropanol). The third region is where structures with well-defined shapes can be obtained, corresponding to the optimized laser power and pixel dwell time. If power is increased further, then structures may be burnt due to a tightly focused laser beam. For practical concerns, it is better to use lower laser power and shorter dwell time. High laser power and long dwell time may result in burnt structures, while too low power or too short dwell time cannot initiate the polymerization process.

For LCEs, two other polymerization regions are observed. In the first region represented in blue color, the polymerized structure dissolves and fades away as time passes. In Figure 4.2, picture (a) shows a reasonably good polymerized structure. Ten seconds later, the structure looks

¹ Colors are used in characterization figures latter in the chapter.

distorted, as shown in b. About two minutes after polymerization, the structure is dissolved. If the power is higher than the fading region, then the polymerized structure does not fade, but rather stays distorted. This is shown in Figure 4.2 c and d.

Figure 4.1: Polymerization regions. (a) No polymerization. (b) Partial Polymerization. (c) Polymerization. (d) Burn.

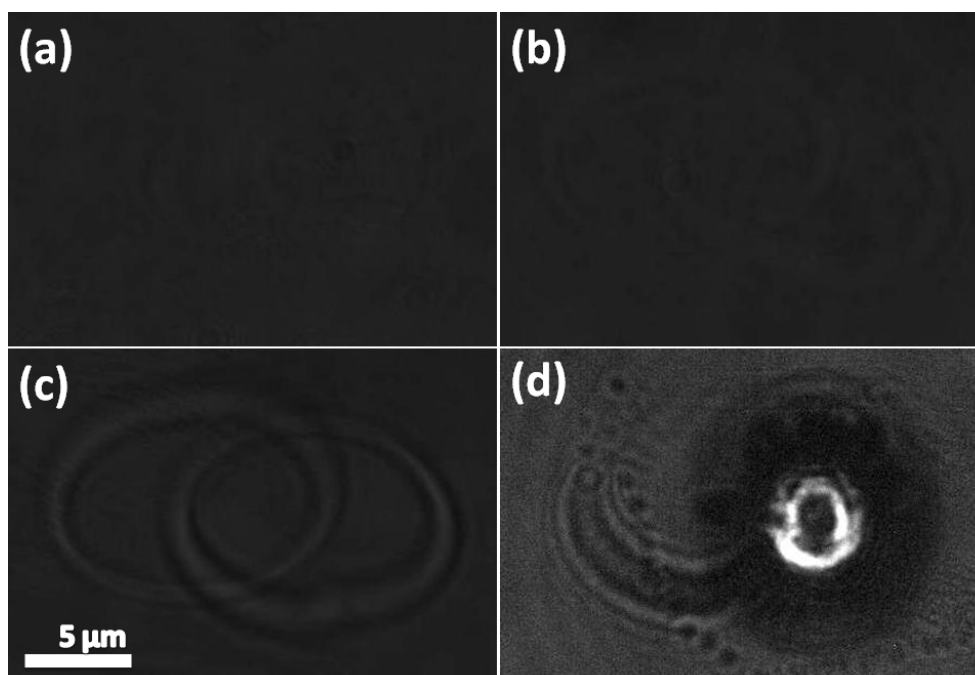
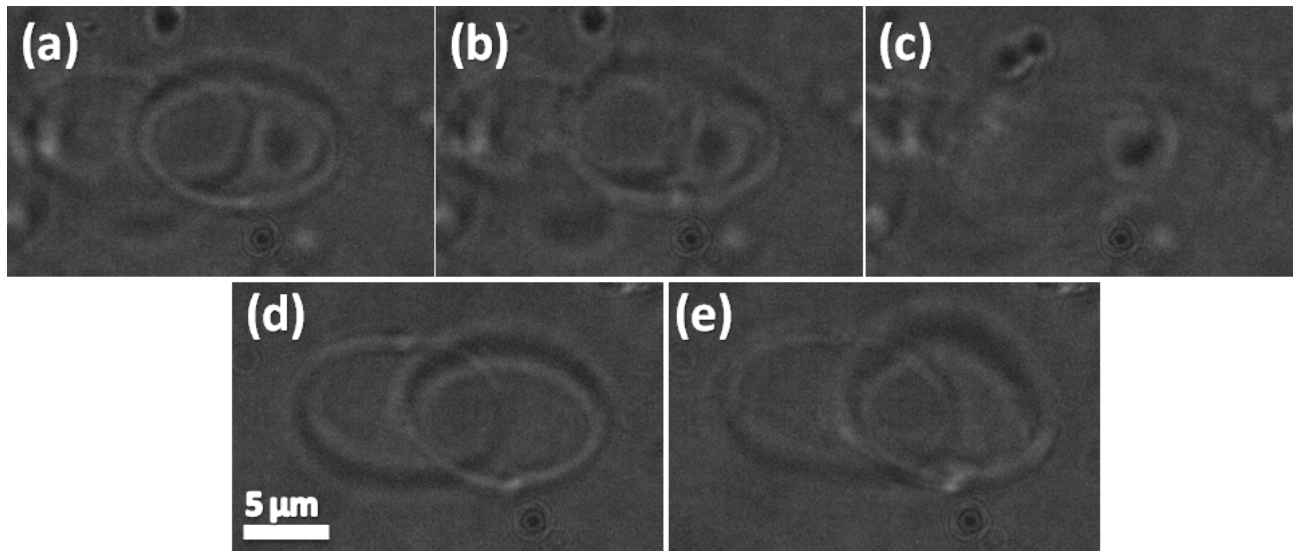


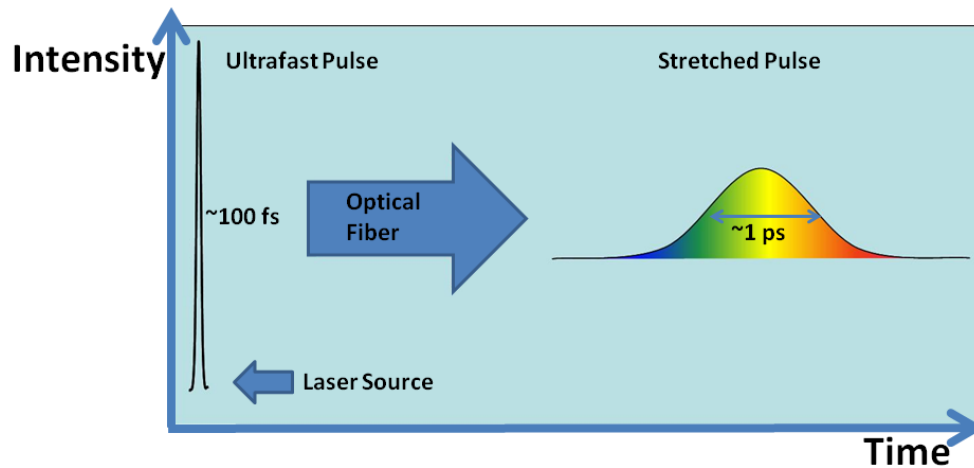
Figure 4.2: Polymerization regions for LCEs: (a) Fading region (right after polymerization). (b) Fading region (10 seconds after polymerization). (c) Fading region (two minutes after polymerization). (d) Distorted region (right after polymerization). (e) Distorted region (10 seconds after polymerization).



4.1 Polymerization with Stretched Pulse

Pulse is stretched by introducing optical fiber. It is changed from a femtosecond to a picosecond pulse. When a pulse stretches, it changes in the temporal scale from a narrow high intensity pulse to a wide low intensity pulse. This is expected to affect polymerization significantly.

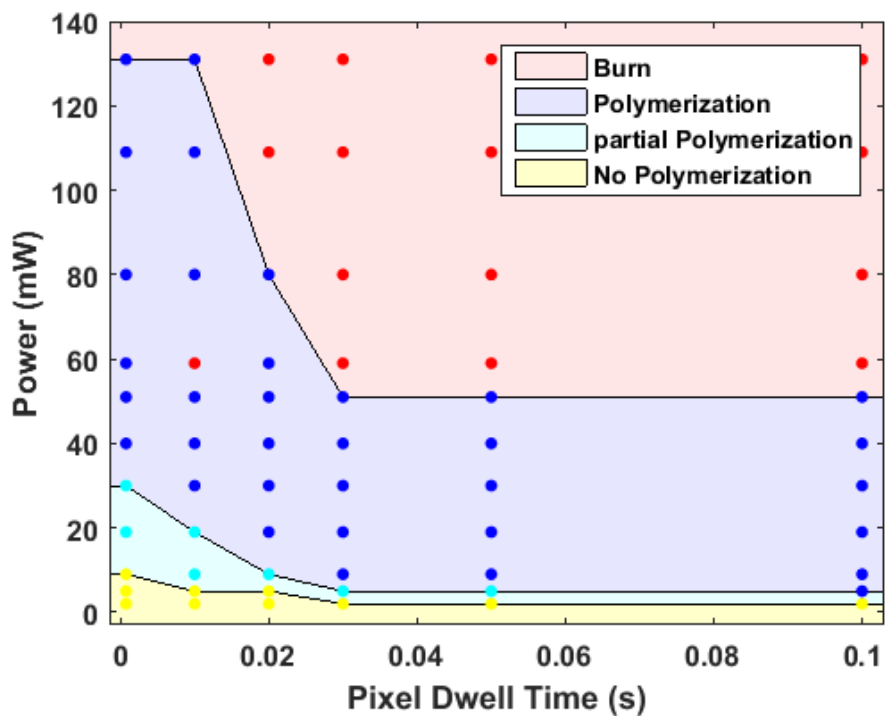
Figure 4.3: Stretched pulse [13].



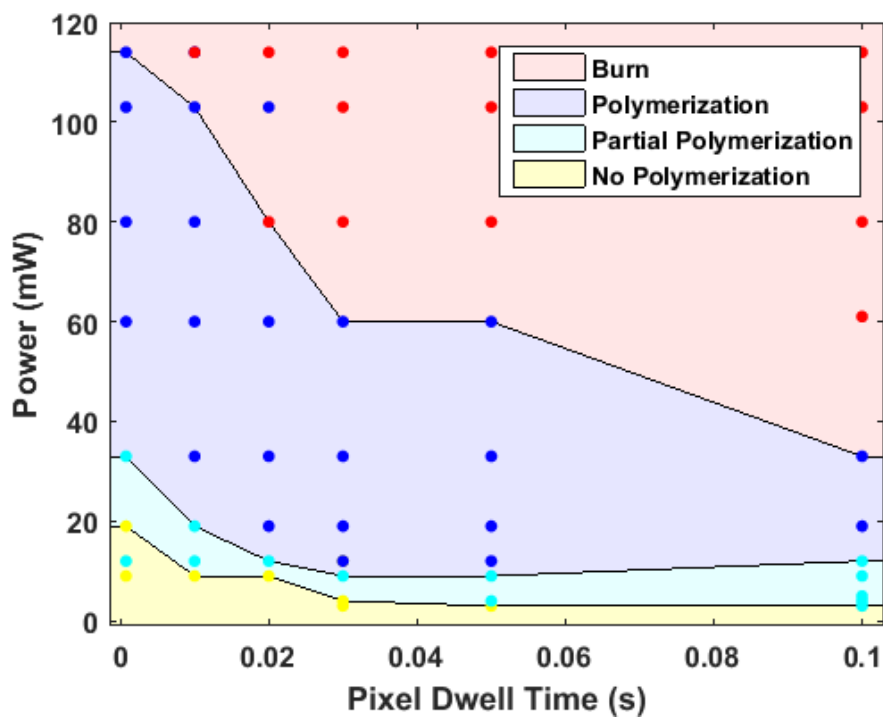
Polymerizable material used for this characterization is Formlabs resin. Two concentrations of photo-initiators are considered: 2% and 4%. Hopf links are 3D printed with speeds defined by Table 3.1. The considered power range is from 2 mW to 140 mW. The power is measured right before the beam hits the dichroic mirror shown in Figure 3.4a. The pixel dwell time is 0.00075-0.1 second.²

The 2% Formlabs resin shows that there are four polymerization regions stacked on top of each other (see Fig. 4.4a). Generally, it is found out that good polymerization happens when a laser power between 30-120 mW is used. Each one of the four regions decreases as exposure time increases. For pixel dwell times that are above 0.03 s, there is not too much change in the behavior of the polymerization regions, and it seems that powers have saturated. There is no fundamental change for 4% Formlabs resin compared to the 2% resin. There is, however, a slight detected decrease in polymerization threshold for 4% Formlabs. This is expected since increasing photo-initiator percentage would increase polymerization.

² Please note that the smallest pixel dwell time in all of the figures is 0.000075 s, not to be confused with zero.



(a) Formlabs polymerization with 2% photo-initiator (stretched pulse)



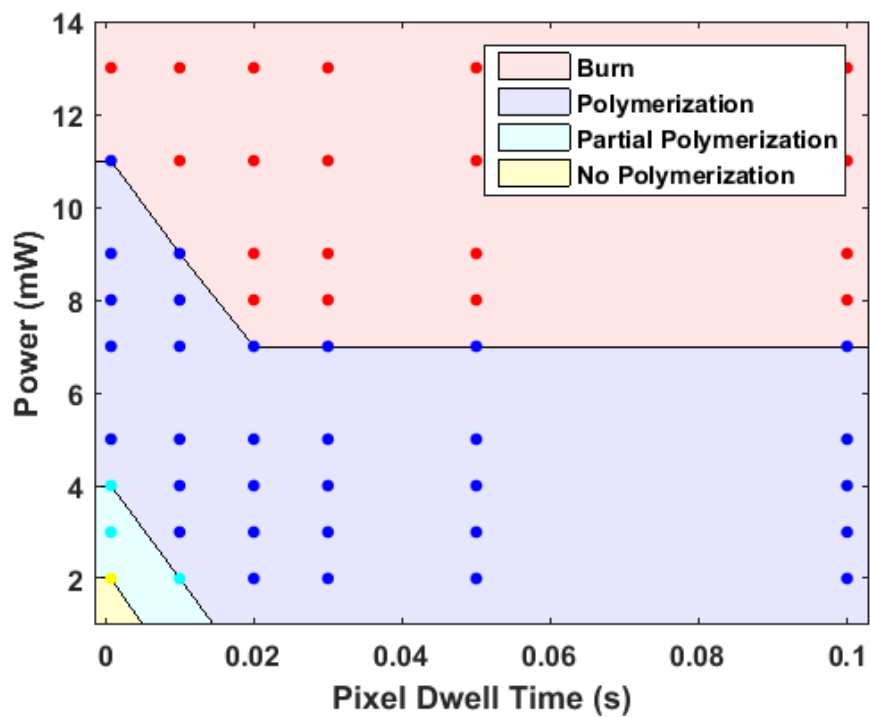
(b) Formlabs with 4% photo-initiator (stretched pulse)

Figure 4.4: Polymerization with stretched pulse.

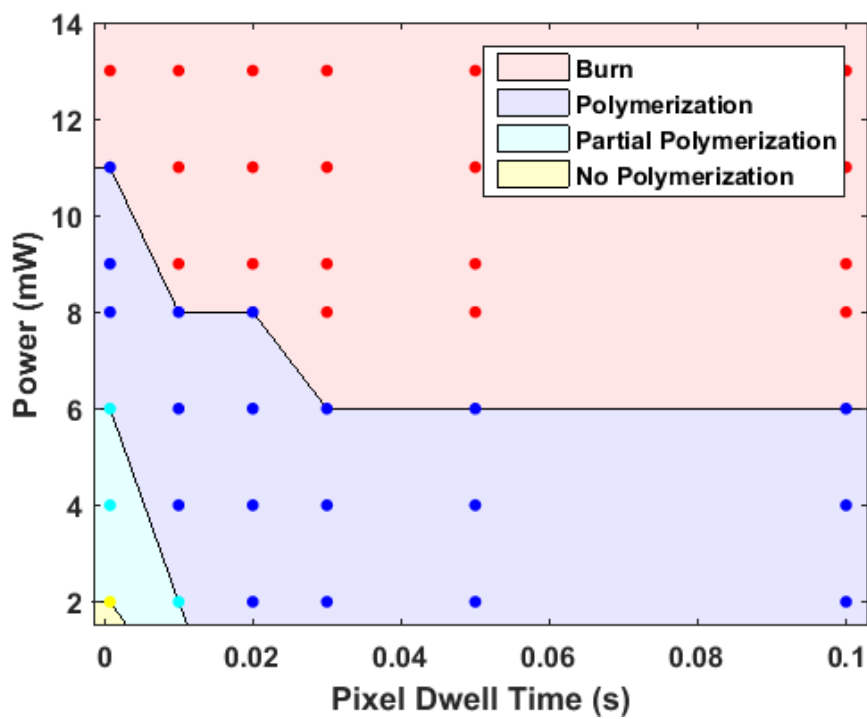
4.2 Polymerization with an Ultrafast Pulse

The optical fiber is removed for this part. The excitation beam used is the original 140 femtosecond beam coming from the Ti-sapphire laser source. One observed significant change is the reduction of power threshold required to polymerize. The regions for no polymerization are almost non-existent. Adding QDs does not significantly affect the polymerization regions of the Formlabs polymerizable material. It shows, however, a decrease in polymerization threshold. The general behavior is similar to that found in polymerization with a stretched pulse. Regions saturates when pixel dwell time is longer than 0.03 second. The range for each region is shorter than in the stretched pulse, and so a small power alteration could affect the quality of the resultant hopf link significantly.

For NOA 63, the regions formation are different than that of Formlabs. For NOA 63, the regions do not saturate after 0.03 seconds. Also, there is no polymerizable region. At 780 nm, NOA 63 is not a good polymerizable material for hopf links.

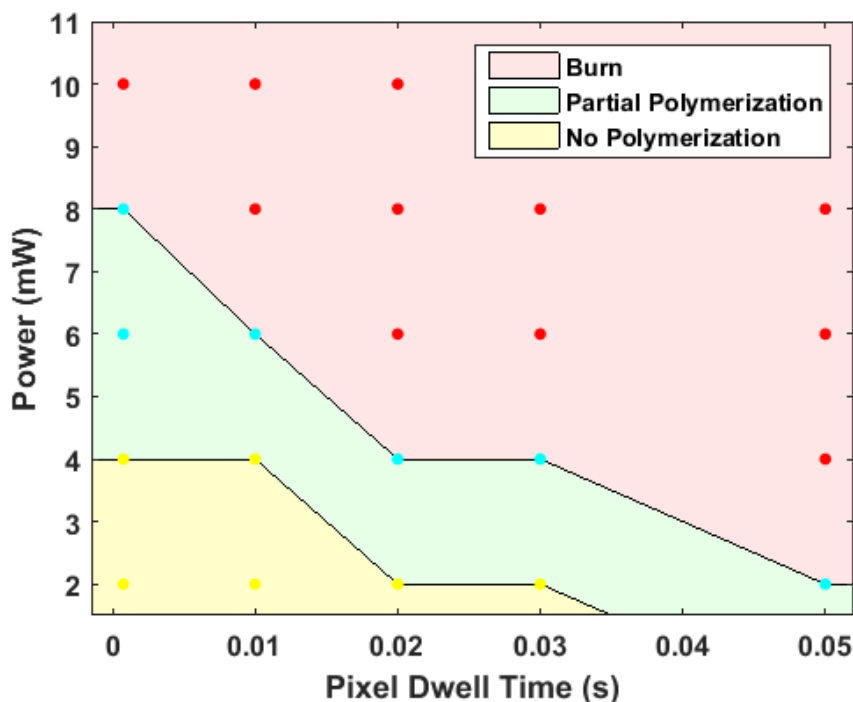


(a) Formlabs with 4% photo-initiator



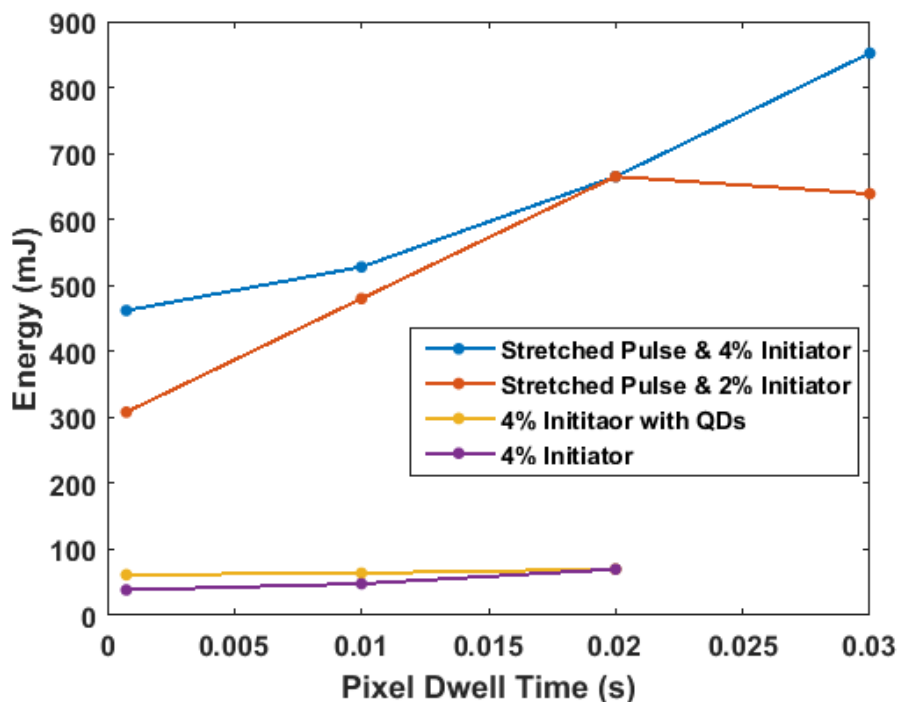
(b) Formlabs with 4% photo-initiator and with quantum dots composites

Figure 4.6: NOA 63 polymerization



To obtain a better understanding of polymerization threshold, required polymerization energy is taken into account. Energy is calculated as $E = P \times t$ where P is power and t is measured dwell time as described in Table 3.1, not program settings dwell time. The reason for this choice is that this is the actual time a laser is focused in the sample. Figure 4.7 shows how energy threshold evolves as a function of pixel dwell time. The points taken to generate this figure are the lower blue points on the corresponding plots. Saturated points are ignored because if a structure is already polymerized, addition of energy would not change the energy threshold. This calculation is a rough estimate for the energy threshold since the points that construct this plot are taken from a finite measured values. There is roughly a factor of ten between energy threshold for stretched pulse and regular pulse.

Figure 4.7: Energy threshold



4.3 Composite Polymerization with Cadmium Telluride Quantum Dots

Before investigating cadmium telluride (CdTe) QDs optical response, a characterization of Formlabs resin fluorescence is carried out to investigate whether or not the optical response is coming mainly from QDs. Figure 4.8 shows that Formlabs resin fluorescence is significantly less than that of Formlabs resin with QDs dispersion. The setup used here is described by Figure 3.2d. Nonetheless, the fluorescence of the resin is greater than that of background noise. This result suggests that Formlabs resin indeed has a fluorescence response, but it is trivial compared to the QDs fluorescence.

Figure 4.9 shows Hopf links with QDs composites under bright field and emission measurement setup described by Figure 3.2d. These pictures are taken after washing the unpolymerized material with isopropanol. This suggests that QDs can be fixed inside hopf links polymerized struc-

tures, and it establishes that the optical properties of QDs are well maintained after dispersing them in polymerized structure.

To quantify the optical response of CdTe inside hopf links, emission spectrum is measured (see fig. 4.10). Before polymerization, the spectrum of QDs and QDs in resin are almost the same. This suggests that the mere introduction of resin does not change the spectrum by a large amount. The spectrum is centered around 700 nm and full width at half maximum (FWHM) of 83.04 nm. The spectrum of QDs in hopf link after polymerization and washing unpolymerized parts is centered around 675 nm, and has a FWHM of 71.91 nm. The spectrum is blueshifted and compressed compared to that of only CdTe QDs. The slight change of the refractive index due to polymerization may be responsible for the shift in the emission spectrum for polymerized hopf links. The size of the QDs could have been altered as well during the polymerization process, resulting in a shift in the spectrum.

Figure 4.8: Resin fluorescence

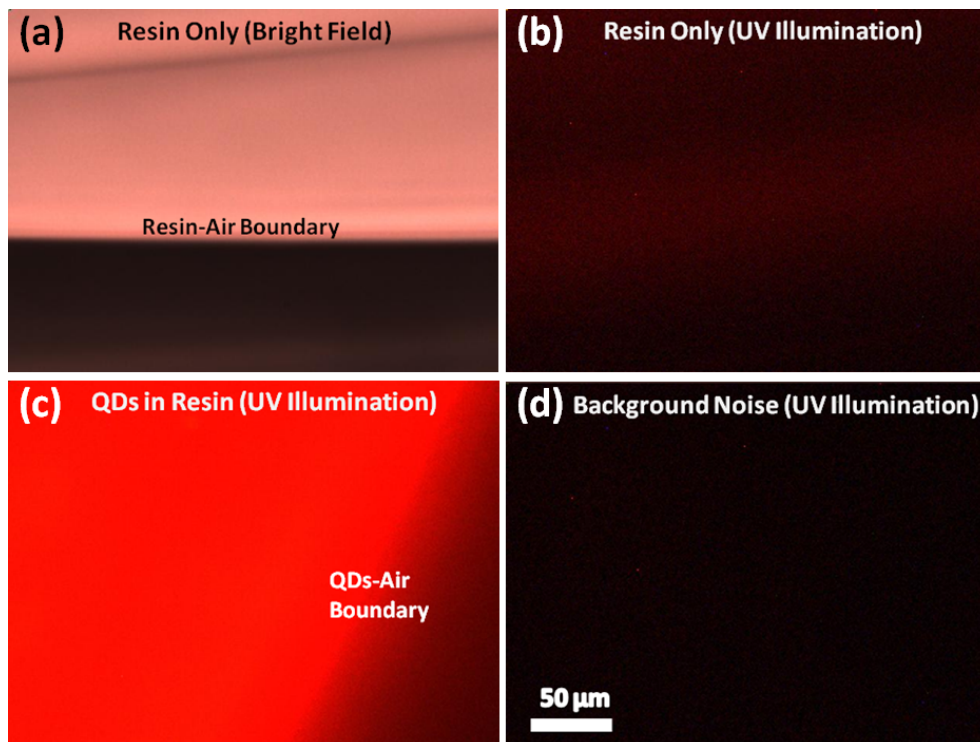


Figure 4.9: QDs fluorescence. (a),(b), and (c) are bright field pictures of the hopf links in (d),(e), and (f) respectively.

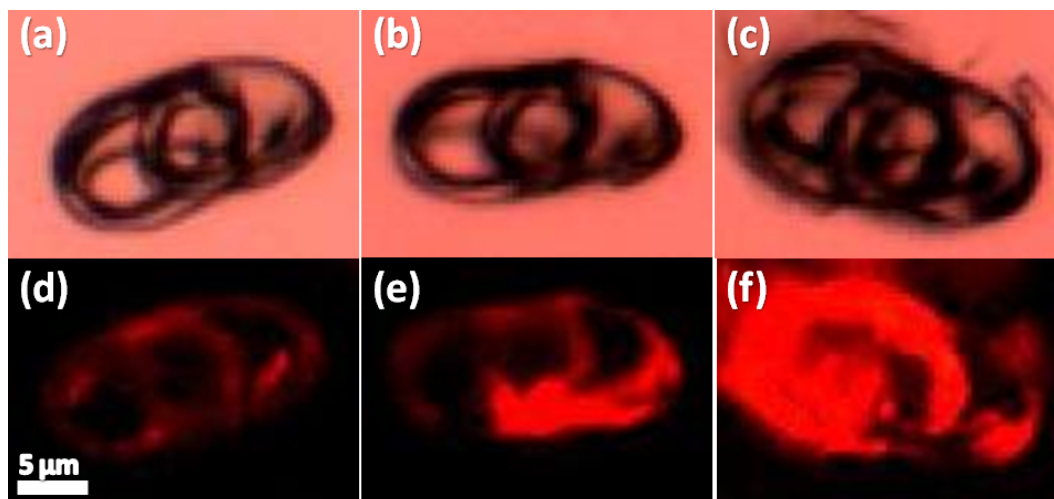
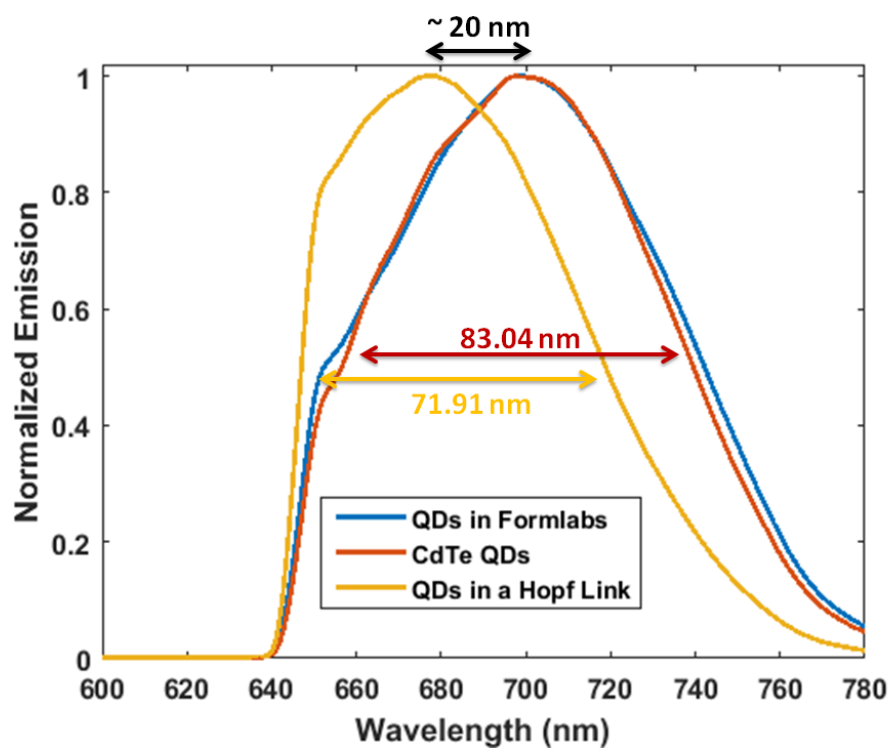


Figure 4.10: Emission spectra



4.4 Elastomer Polymerization

4.4.1 Preparation

A mixture of monomers, cross-linker and photo-initiator is used to obtain LCE structures. This mixture is confined in a cell. The cell is first heated to 85°C then cooled naturally to a lower temperature, during which the mixture undergoes transition from isotropic phase to LC phase. The orientation of LC molecules is defined by the homeotropic BCs imposed on both the glass substrate and cover glass. Relaxation of the molecules can be checked under polarizing microscopy. Use of red filter is required to prevent polymerization. To quantify how much LCEs are aligned, the alignment percentage is calculated by counting the number of black pixels in an image, and then dividing by the total number of pixels. It is done in Matlab. To test the threshold condition chosen for black pixel, images of black and yellow backgrounds are passed to the program, and it returned 92.53% and 6.32% respectively. This result validates the program.

Right after the phase change, the LCEs look as in Figure 4.11a. The relaxation of LCEs right after they have gone through the phase change and the heating stage is turned off is shown in Figure 4.11. The pictures span a 20 hour period. Black regions represent areas where LCEs are aligned, and yellow regions represent areas where the orientation of LCEs is not homeotropically aligned. Alignment is plotted for this relaxation (fig. REFres lc Label). Alignment seems to increase as time advances. However, the alignment rate does not increase by a lot for the most time.

To stimulate alignment, the heating stage was turned on and set at about 43°C . Figure 4.12 shows alignment relaxation overnight. There is a significant jump that occurred when the heating stage was turned on again. The overall increase in alignment that is achieved is about a factor of two.

Figure 4.11: LCEs heated over night. (a) Heating stage turned off from 85°C . (b) Just before turning heating stage back on to 43°C . (c) Just after turning on heating stage to 43°C . (d) Three hours after turning the heating stage on. (e) Four hours after turning the heating stage on. (f) 17 hours after turning the heating stage on.

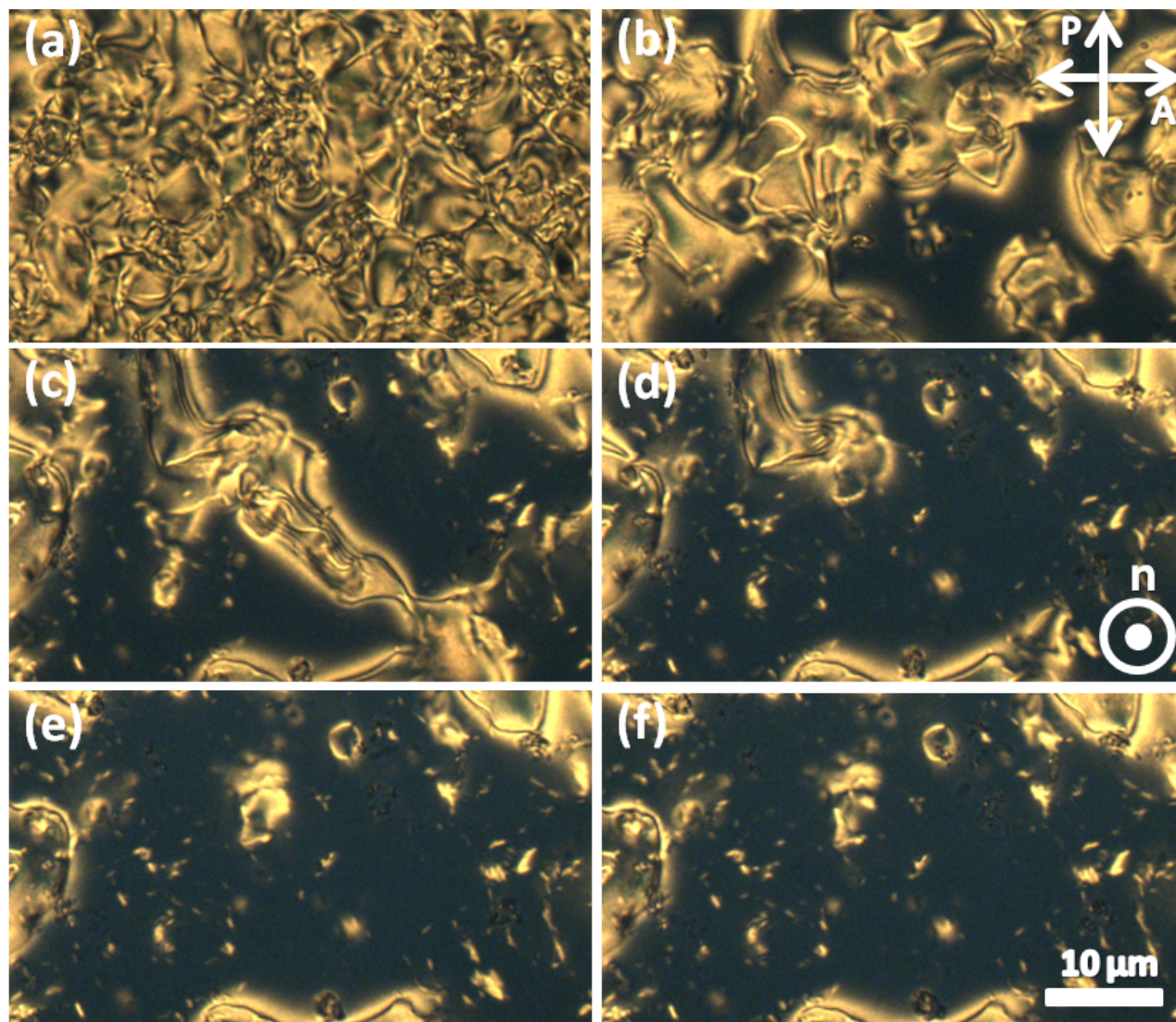
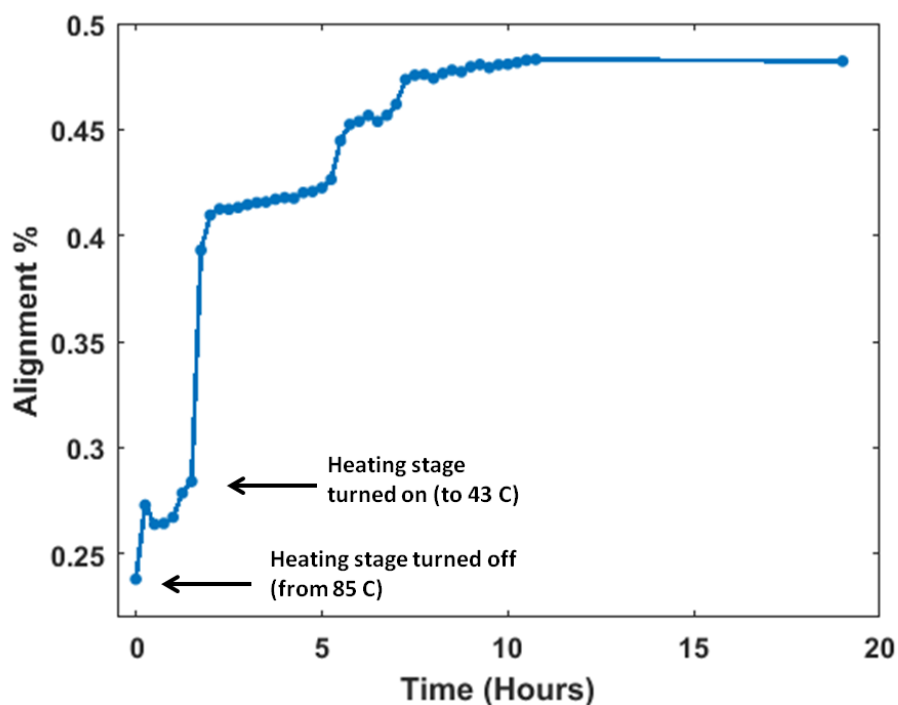


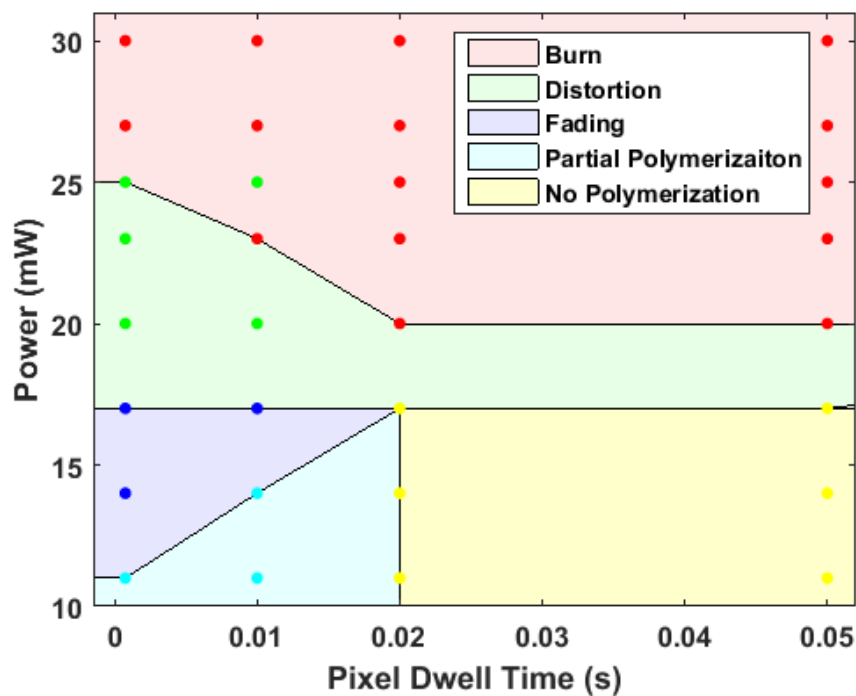
Figure 4.12: LCE overnight alignment. First jump is due to turning the heating stage back on to 43°C . The second jump is due to a sudden change in orientation that happened in the sample. Specifically, it is what happened between Fig.4.11 (c), (d), and then (e).



4.4.2 Experiment

Although the samples prepared are not perfect, there are sufficient aligned areas to do 2PP. The polymerization regions for LCEs are the most complex among those considered. There are five regions. There is the usual burn and partial polymerization regions. There is a region of fading polymerization. Another new area is distortion region. The no polymerization region is placed differently than usual. It occurs for low energy and high speeds. By the time the structure is printed, the hopf link has already faded, marking a no polymerization region. A "good" polymerization region does not exist here. This is due to the fact that this material is too soft. When a structure is polymerized, it distorts and dissolves.

Figure 4.13: LCE polymerization regions. Distortion and fading regions are explained in Fig.4.2.



In comparison to Formlabs polymerizable material, LCEs require higher polymerization powers. The polymerized structure is also more fragile and could easily distort or dissolve. The range for polymerization is about the same for both materials at 7.5 ms. LCE polymerized hopf links are anisotropic, while those of Formlabs are isotropic.

Chapter 5

Conclusions

In order to study two-photon polymerization of composites in soft matter systems, we have studied polymerization of polymerizable resin, polymerizable resin doped with quantum dots, and liquid crystal elastomers.

To understand fundamentally how the pulsewidth of laser pulses has an effect on the non-linear nature of 2PP. We studied 2PP with pulses stretched by a five-meter-long single mode fiber from pulsewidth of 150 femtoseconds to a couple picoseconds. Higher power is required for 2PP with stretched pulses.

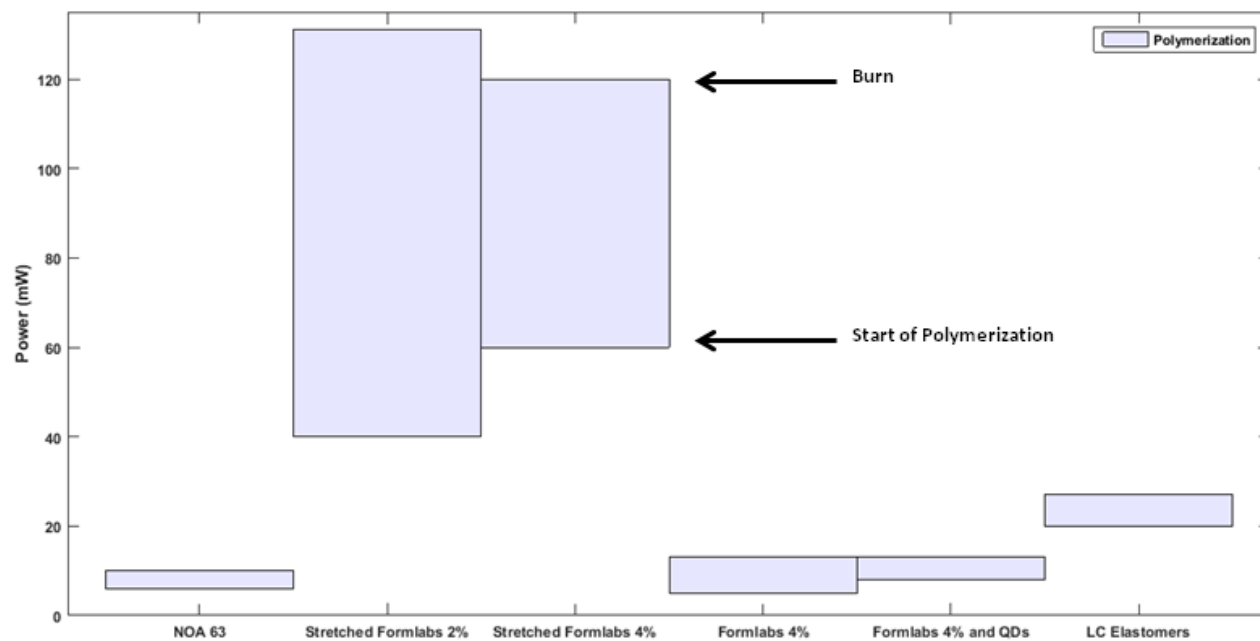
We characterize the polymerizable parameter region based on laser power and pixel dwell time (Fig. 5.1). Comparing these regions between polymerizable resin and resin doped with quantum dots, we do not find significant differences. However, the polymerization region for resin doped with quantum dots extends slightly, indicating slight lowering of the energy fluence threshold for polymerization. The physics behind this lowering of threshold needs to be further investigated. It would certainly be a direction for future work to explore how the inclusion of nanoparticles affect polymerization threshold of the composites.

The optical response of polymerized microparticles with quantum dot inclusions clearly evidences successful fabrication of composite particles with engineered optical properties. These particles show strong fluorescence under UV illumination which resembles that of the included quantum dots, but with a blueshifted emission peak and a narrower bandwidth. One potential future work could be improving the quantum dot and monomer mixture by direct grafting of monomers to

quantum dots [32]. Fabrication of microparticles in LCEs by 2PP is also achieved, though the energy threshold for polymerization is higher than other material (Fig. 5.1). By heating the sample overnight, the orientational alignment is improved and writing of particles can be done by 2PP in the aligned region.

In short, we have achieved composite microparticles with nanoparticle inclusions exhibiting properties closely resemble those of the included nanoparticles. Microparticles with mechanical properties depending on temperatures are also studied with liquid crystal elastomers. These properties can be engineered by selecting different species of nanoparticles. Optical, plasmonic, or even upconverting properties can be pre-engineered and tuned. It is foreseeable that interactions could happen in the same microparticle between different nanoparticles, such as quantum dots/upconversion particles and plasmonic nanoparticles, rendering strong enhancement of optical or upconversion response. Furthermore, It is possible these microparticles with pre-engineered mechanical and optical properties, self-assemble into colloidal crystalline structures and display interesting collective properties. The aforementioned directions, though exciting and of great significance, is beyond the scope of this thesis. We expect to further explore them in future work.

Figure 5.1: Polymerization region for a pixel dwell time of 0.00075 s.



Bibliography

- [1] Mykola Tasinkevych Angel Martinez, Leonardo Hermosillo and Ivan I. Smalyukh. Linked topological colloids in a nematic host. PNAS, 112:45464551, 2015.
- [2] Scott E Fraser Virginia E Papaioannou Anna-Katerina Hadjantonak, Mary Dickinson. Technicolour transgenics: imaging tools for functional genomics in the mouse. Nature Reviews, Genetics, 4:613–625, 2003.
- [3] Krishnan Venkatakrishnan Bo Tan and Alexander Makaronets. Effects of pulsewidth on two-photon polymerization. Designed Monomers and Polymers, 16:2:145–150, 2013.
- [4] Qingkun Liu Mykola Tasinkevych Bohdan Senyuk, Manoj B. Pandey and Ivan I. Smalyukh. Colloidal spirals in nematic liquid crystals. Soft Matter, Issue 45:8758–8767, 2015.
- [5] Stephen Barlow Daniel L. Dyer Jeffrey E. Ehrlich Lael L. Erskine Ahmed A. Heikal Stephen M. Kuebler I.-Y. Sandy Lee Dianne McCord-Maughon Jinqi Qin Harald Rockel Mariacristina Rumi Xiang-Li Wu Seth R. Marder Brian H. Cumpston, Sundaravel P. Ananthavel and Joseph W. Perry. Two-photon polymerization initiators for threedimensional optical data storage and microfabrication. Nature, Vol. 398:51–54, 1999.
- [6] Sven Passinger Carsten Reinhardt and Boris N. Chichkov. Laser-fabricated dielectric optical components for surface plasmon polaritons. Optics Letters, Vol. 31, No. 9:1307–1309, 2006.
- [7] J. Naciri R. Pink H. Jeon D. Shenoy D. L. Thomsen III, P. Keller and B. R. Ratna. Liquid crystal elastomers with mechanical properties of a muscle. MACROMOLECULES, 34:5868–5875, 2001.
- [8] Michael W. Davidson. Fundamentals of mercury arc lamps. Zeiss, Florida State University.
- [9] Thomas J. Fellers Michael W. Davidson Douglas B. Murphy, Kenneth R. Spring. Principles of birefringence. Microscopy, 2008.
- [10] Formlabs. Materials data sheet. Formlabs webpage, 2016.
- [11] Derek Gann. Raman signal enhancement for low-noise, chemically sensitive imaging in soft matter systems. CU Scholar, Paper 98, 2014.
- [12] M. A. Greenwood. Photonics, 2007.
- [13] G. M. Greetham. Amplitude technologies. Product Imaging and Correlation: Non-adiabatic Interactions in Chemistry (PICNIC).

- [14] D. G. Hasko J. Gorman and D. A. Williams. Charge-qubit operation of an isolated double quantum dot. Physical Review Letters, Vol. 95, Iss. 9:090502, 2005.
- [15] A. Ostendorf B. N. Chichkov R. Houbertz G. Domann J. Schulz C. Cronauer L. Frhlich J. Serbin, A. Egbert and M. Popall. Femtosecond laser-induced two-photon polymerization of inorganicorganic hybrid materials for applications in photonics. Optics Letters, Vol. 28, No. 5:301–303, 2003.
- [16] Vijay Bhooshan Kumar K. Santhosh Kumar and Pradip Paik. Recent advancement in functional core-shell nanoparticles of polymers: Synthesis, physical properties, and applications in medical biotechnology. Journal of Nanoparticles, 2013:672059, 2013.
- [17] Wolfgang Ketterle. Two-Photon Excitation. MIT Center for Ultracold Atoms, 2006.
- [18] Marta Lavri. Liquid crystal elastomers. Jozef Stefan Institute, 2011.
- [19] Nan Zhang Yuliang Zhang Zheng Fang Weihong Zhu Lei Zou, Zhenyu Gu and Xinhua Zhong. Ultrafast synthesis of highly luminescent green- to near infrared-emitting cdte nanocrystals in aqueous phase. Materials Chemistry, 18:2807–2815, 2008.
- [20] Y. Yuan D. Konetski I. I. Smalyukh M. Podgrski, C. Wang and C. N. Bowman. Pristine polysulfone networks as a class of polysulfide-derived high-performance functional materials. CHEMISTRY OF MATERIALS, 28:5102–5109, 2016.
- [21] M. A. McEvoy and N. Correll. Materials that couple sensing, actuation, computation, and communication. Journal of Nanoparticles, 347:1261689, 2015.
- [22] PlasmacChem. Quantum dots. PlasmaChem Webpage, 2012.
- [23] Norland Products. Norland optical adhesive 63. Norland Products webpage.
- [24] Stephanie A. Pruzinsky and Paul V. Braun. Fabrication and characterization of two-photon polymerized features in colloidal crystals. Advanced Functional Materials, 15:19952004, 2005.
- [25] Sein Leung Soo Christoph Nobel Helmi Attia Gregor Kappmeyer Serafettin Engin Rachid MSaoubi, Dragos Axinte and Wei-Ming Sim. High performance cutting of advanced aerospace alloys and composite materials. CIRP Annals - Manufacturing Technology, 64:557–580, 2015.
- [26] Derryck Reid. Nonlinear semiconductor microscopy. Ultrafast Optics Group at Heriot Watt University, 2008.
- [27] B. Senyuk. Liquid crystals: a simple view on a complex matter. Kent university webpage.
- [28] Osamu Nakamura Shoji Maruo and Satoshi Kawata. Three-dimensional microfabrication with two-photon-absorbed photopolymerization. Optics Letters, Vol. 22, No. 2:132–134, 1997.
- [29] S. Geyer K. MacLean M. G. Bawendi T. S. Mentzel, V. J. Porter and M. A. Kastner. Charge transport in pbse nanocrystal arrays. Physical Review B, 77:075316, 2008.
- [30] Rahul P. Trivedi Taewoo Lee, Bohdan Senyuk and Ivan I. Smalyukh. Optical microscopy of soft matter systems. Cornell University Library (ArXiv), 1108.3287, 2011.

- [31] L. A. Bentolila J. M. Tsay S. Doose J. J. Li G. Sundaresan A. M. Wu S. S. Gambhir X. Michalet, F. F. Pinaud and S. Weiss. Quantum dots for live cells, in vivo imaging, and diagnostics. Science, Vol. 307, Issue 5709:538–544, 2005.
- [32] Jrme Plain Safi Jradi Xiao Wei Sun Hilmi Volkan Demir Xuyong Yang Claire Deeb Stephen K Gray Gary P Wiederrecht Xuan Zhou, Olivier Soppera and Renaud Bachelot. Plasmon-based photopolymerization: near-field probing, advanced photonic nanostructures and nanophotocchemistry. Journal of Optics, 16, 2014.
- [33] Bohdan Senyuk Mykola Tasinkevych Ye Yuan, Angel Martinez and Ivan I. Smalyukh. Effects of chirality on elastic interactions and colloidal self-assembly in nematic liquid crystals. In manuscript, 2017.
- [34] A. D. Yoffe. Semiconductor quantum dots and related systems: Electronic, optical, luminescence and related properties of low dimensional systems. Advances in Physics, 50:1–208, 2001.